



Assessing the influence of rooftop vegetation on pollution dispersion in urban canyons through Large-Eddy Simulations

Malik Safi Ullah¹*, Alessandro Di Giulio, Carlo Cintolesi, Silvana Di Sabatino

Department of Physics and Astronomy "Augusto Righi", University of Bologna, via Irnerio 46, 40126, Bologna, Italy

ARTICLE INFO

Keywords:

Green nature-based solutions
Pollutant dispersion
Turbulence
Large-Eddy Simulation
OpenFOAM
Urban canyon

ABSTRACT

Urban air pollution is a significant hazard to human health, which is expected to worsen with the increase of urbanisation worldwide. There is a growing need to evaluate mitigation measures such as green Nature-Based Solutions. However, most studies focus on vegetation at street level, while the role of rooftop trees remains largely unexplored. Here, we investigate a simplified urban canyon where trees are placed on building rooftops, at the canyon-atmosphere interface level, which is a key area for pollutant removal mechanisms. Nine types of tree crown are analysed using highly-resolved Large-Eddy Simulations at Reynolds number $Re = 2 \times 10^4$. The simulation without trees is successfully validated against laboratory and numerical experiments. Results show that the key parameter is the tree crown density, while other characteristics like the leaf area index play a secondary role. Overall, rooftop trees reduce horizontal velocity and increase the turbulent kinetic energy (TKE) in the outer layer above the canyon: low-density-crown trees generate higher TKE, mimicking the presence of isolated obstacles and increasing the turbulent vertical mixing; high-density-crown trees reduce the atmospheric wind velocity, mainly acting as an extended area of momentum sink, which also reduces the wind turbulent level. Within the canyon, rooftop trees have a limited effect on the overall dynamics and the pollutant concentration distribution. Hence, unlike street trees, rooftop trees can be used to extend urban green areas and shade streets without hampering the dispersion of pollutants.

1. Introduction

Air pollution poses an alarming threat to human health, particularly in urban areas where the level of pollutants tends to exceed normal standards (Ortiz and Guerreiro, 2020). This is of particular concern considering that a large and increasing share of the global population lives in urban areas (World Health Organization, 2025; Santiago et al., 2022). Growing awareness of the health hazards posed by air pollution has also generated huge research efforts devoted to effective measures to reduce pollution exposure and promote healthier living conditions in urban areas (Moradpour and Hosseini, 2020). Among these, Nature-Based Solutions (NBS) are increasingly recognised as effective strategies for mitigating air pollution in urban environments. Vegetation, particularly trees and green areas, bioretention systems, and constructed wetlands, plays a crucial role in pollutant dispersion by acting as a physical barrier, enhancing deposition, and promoting pollutant uptake. These NBS can improve air quality by filtering particulate matter (PM10 and PM2.5) and absorbing gaseous pollutants through plant surfaces and soil microbial interactions. Additionally, vegetation barriers can facilitate airflow patterns, enhancing pollutant dispersion and dilution, thereby reducing localised concentrations of harmful pollutants (Biswal et al., 2022).

* Corresponding author.

E-mail address: maliksafi.ullah2@unibo.it (M.S. Ullah).

<https://doi.org/10.1016/j.uclim.2025.102614>

Received 18 July 2025; Received in revised form 26 August 2025; Accepted 12 September 2025

Available online 20 September 2025

2212-0955/© 2025 The Author(s). Published by Elsevier B.V. This is an open access article under the CC BY license (<http://creativecommons.org/licenses/by/4.0/>).

Pollutant dispersion in urban environments has been widely investigated in relation to different urban geometries and flow scenarios, including street canyon configurations, open spaces, and complex building arrays. At the city scale and in the absence of vegetation, [Byoungchull and Beungyong \(2024\)](#) assess the effects of urban morphology on pedestrian-level ventilation utilising the standard $k-\epsilon$ model. They found that staggered or asymmetrical building disposition improved ventilation and pollutant dispersion, whereas denser, grid-like configurations led to elevated pollutant levels owing to decreased airflow from a canyon. [Di Sabatino et al. \(2018\)](#) discussed the interaction between meteorological conditions and urban morphology on the dispersion of pollutants, while [Baratian-Ghorghi and Kaye \(2013\)](#) analysed the influence of urban canyon aspect ratio on the removal of dense pollutants from streets. They found that narrow canyons cause stronger stratification, making pollutant removal slower. The limited space weakens air circulation, causing pollutants to stay longer. Conversely, wider canyons help remove pollutants more effectively by creating stronger upward and downward air movements. [Gurjão et al. \(2024\)](#) emphasise the role of urban planning, including green corridors and strategic infrastructure design, in mitigating pollution and improving air quality, while [Nosek et al. \(2025\)](#) examines the ventilation performance of deeper street canyons and a variety of roof geometries, with the finding that canyons with greater depth, an aspect ratio of two and pitched roof inherently enhance pollutant removal because of a better lateral and vertical advection. [Cintolesi et al. \(2021\)](#) use LES to study how rooftop alterations affect pollution dispersion in urban canyons. The study found that adding impediments to rooftops increases mixing and turbulence, lowering pollution concentrations by 34% for flat roofs.

The introduction of green NBS, like street trees or green areas, is considered a passive measure in removing pollutants from an urban canyon, having additional co-benefits in terms of mitigating temperature extremes and increasing the city's livability and citizens' well-being. [Tallis et al. \(2011\)](#) estimated that London's urban tree canopy removes PM10 at an annual rate of 852–2121 tonnes, equivalent to approximately 0.7–1.4% of PM10 in the urban boundary layer. Increasing tree areas from 20% to 30% in the year 2050 would move the removal up to 1109–2379 tons a year. [Irga et al. \(2015\)](#) demonstrate that urban forestry is associated with significant reductions in PM10 and PM2.5 levels in high-density vegetation areas of Sydney, Australia. [Wang et al. \(2022\)](#) observed that urban trees influence the climate through shading, evapotranspiration, and wind resistance, with higher Leaf Area Index (LAI) and larger crown of trees show an increase in heat transfer to latent heat, and with sparse planting densities providing improved cooling. [Ghasemian et al. \(2017\)](#) study the impact of solid and vegetation barriers on the roadside using the RANS technique coupled with the realisable $k-\epsilon$ turbulence model. Solid barriers improve air quality by inducing upward airflow, lifting pollutant plumes, and reducing ground-level concentrations by 58%. Vegetation barriers showed mixed effects depending on their density; dense canopies with high Leaf Area Density ($LAD = 3.33$) improved air quality by 10% through vertical mixing, while high-porosity canopies ($LAD = 1$) worsened air quality by 15% due to pollutant stagnation. [Balczó et al. \(2009\)](#) investigated the impact of LAD on pollutant concentrations using the RANS numerical model, while [Gromke and Blocken \(2015b\)](#) examined the effect of trees in street canyons by employing the RANS standard $k-\epsilon$ model and the Reynolds Stress Turbulence (RST) model. Both studies concluded that the presence of trees in avenue canyons generally leads to increased pollutant concentrations due to reduced ventilation. However, findings also indicate that strategically designed street tree arrangements can help in reducing pollutant dispersion, underscoring the need for careful planning to balance the benefits and potential drawbacks of urban vegetation. [Gallagher et al. \(2015\)](#) review passive methods: porous barriers, such as trees and vegetation, and solid barriers like walls and parked cars, for improving air quality in urban environments. The study highlights that barriers can modify the dispersion patterns and lower the concentrations of pollutants, but their effectiveness depends on local geometry and meteorological conditions. [Abhijith and Gokhale \(2015\)](#) investigate the passive control potential of trees and on-street parked cars in reducing air pollution in urban street canyons. The study demonstrates that medium-sized trees with high porosity and low density, combined with parallel or perpendicular automobile parking arrangements, limit pedestrian exposure to pollutants. However, high density of trees and angled parking have been found to impede airflow, leading to localised pollutant accumulation. [Gromke and Blocken \(2014\)](#) utilised the RANS simulation with the RST model to reproduce an idealised urban neighbourhood, demonstrating that the strategic placement of trees along avenues or the establishment of parks significantly reduces pollutant concentrations. Similarly, [Jeanjean et al. \(2015\)](#) used $k-\epsilon$ turbulence model for the analysis in the neighbourhood of Leicester City Centre, finding that the aerodynamic influence of trees contributes to an approximate 7% reduction in normalised pedestrian-level pollutant concentrations. [Zhang et al. \(2021\)](#) investigated the impact of green roof systems on airflow dynamics and pollutant dispersion within urban street canyons of varying geometries and thermal stratifications. The study found that the placement of green roofs on both windward and leeward sides enhances pollutant removal by modifying wind flow patterns and generating regions of increased air circulation, particularly in tall canyons with an aspect ratio ($AR = H/W$) greater than or equal to 2 ($H/W \geq 2$). Here, H represents the building height, and W represents the street width. The findings further emphasise that green NBSs (including tree canopies, vegetative barriers, and rooftop trees) improve urban air quality by promoting vertical mixing, facilitating pollutant dispersion, and altering airflow structures.

Focussing on the use of trees as NBSs, their effectiveness largely depends on tree type, crown morphological characteristics, and planting distribution, which mainly affect the air dynamics in the urban canopy. [Shen et al. \(2023\)](#) highlight the importance of tree planting distribution in affecting pollutant dispersion, emphasising that an optimised distribution can lead up to a 37% reduction in pollutant concentrations. [Ren et al. \(2023\)](#) found that medium tree spacing, where crown diameter is proportional to planting distance (approximately 14 m), attenuates more than 50% of PM exposure for pedestrians and cyclists. [Chen et al. \(2021\)](#) demonstrate that trees with high LAD effectively reduce Total Suspended Particles and PM10, when integrated with shrubs and herbs. They also highlight that dense tree canopies can impede wind flow, altering airflow patterns and pollutant dispersion dynamics. [Guo et al. \(2023\)](#) examine the influence of tree morphological characteristics (including LAD, crown diameter, and trunk height) on pollutant dispersion in urban canyons. The study finds that trees with a moderate LAD of approximately 1.5 and an appropriately sized crown diameter of about six metres enhance airflow and pollutant removal, particularly in canyons with low aspect ratios. While urban vegetation includes diverse plant species with varying morphological characteristics, most studies have

not examined the combined effects of factors such as crown diameter, LAD, and LAI on pollutant dispersion within a single study, highlighting a gap in existing research.

A few studies on this topic have employed LES for turbulence modelling, providing higher accuracy in capturing transient pollutant dispersion patterns. While most literature discusses RANS simulations, LES remains a good approach due to its ability to resolve small-scale turbulence and enhance the understanding of airflow dynamics in urban environments. While LES is well-suited for capturing unsteady turbulent structures, it remains computationally intensive and sensitive to modelling assumptions, including domain size, boundary conditions, and subgrid-scale parameterisations (Tominaga and Stathopoulos, 2013). Cintolesi et al. (2021) applied LES to study how building surface conditions influence pollutant dispersion, showing that façade heating can significantly modify airflow and vortex strength within an urban canyon. Although the study focuses on thermal effects rather than vegetation, the results underscore LES capability in resolving complex urban-scale flow interaction and transient pollutant dynamics. Salim et al. (2011) compare LES and RANS models in predicting pollutant dispersion within urban environments. While RANS model, particularly the RST model, provides reasonably accurate mean concentration predictions, LES demonstrates good performance by capturing unsteady mixing events critical for street canyon ventilation. Ono and Nozu (2024) evaluate the performance of LES against wind tunnel measurements for modelling pollutant dispersion in a densely populated urban district. The study finds that LES accurately reproduces mean pollutant concentrations and vertical dispersion structures, though minor discrepancies are observed in higher-order concentration moments. McMullan and Angelino (2022) utilise LES to assess the impact of crown porosity and tree density on the dispersion of traffic-related pollutants in urban street canyons. The study finds that tree crowns obstruct canyon vortex ventilation, leading to a threefold increase in pollutant concentrations at pedestrian level along the leeward wall. Wang et al. (2024) evaluate the performance of various turbulence modelling approaches, including steady-state and unsteady-state RANS (SRANS/URANS) with Re-Normalisation Group (*RNG*) $k - \epsilon$ and Shear Stress Transport (*SST*) $k - \omega$ models, alongside LES, in simulating pollutant dispersion within urban street canyons for both generic and real urban layouts. The study finds that LES is the most effective technique for capturing small-scale turbulence, while SRANS/URANS models exhibit limited applicability in complex urban geometries. These findings highlight the effectiveness of LES in analysing transient pollutant dispersion patterns, emphasising the necessity of precise airflow modelling for urban air quality assessments.

While existing studies emphasise the role of urban greenery in mitigating air pollution, several limitations persist. For example, Ren et al. (2023) conducted field measurements and CFD analysis showing the benefits of medium tree spacing, but their study is limited to a single location; Guo et al. (2023) used idealised CFD scenarios but focused only on PM_{10} and neglected practical constraints; and Shen et al. (2023) used CFD modelling to assess mixed vegetation layouts, but considered only perpendicular wind and a single canyon geometry. Most studies rely on RANS-based simulations and do not systematically assess rooftop trees with varying crown characteristics (e.g. radial LAD and global LAI). The present study addresses this gap by systematically analysing how eight types of rooftop trees modify the urban canyon airflow and pollutant dispersion.

Among various green roof options, conventional systems typically incorporate low-growing vegetation such as mosses, succulents, and small herbaceous plants. Nonetheless, there is growing interest in integrating small trees into green roof systems, especially in dense urban environments. Rooftop-compatible tree species, typically ranging from 2 to 5 m in height, include *Syringa vulgaris* cultivars, *Photinia x fraseri*, and *Amelanchier grandiflora*. Rooftop trees are used in various projects, such as the 'Bosco Verticale' in Milan (Italy), which includes tree species on balconies and rooftop (Kalogeropoulos et al., 2024; Di Paola, 2021), and rooftop garden in Dhaka (Bangladesh), which outlines standards for small-tree implementation on intensive green roofs (Safayet et al., 2017). Effect of trees is also subjected to seasonal variability and climatic conditions, as leaf area can strongly influence pollutant removal and aerodynamic effects, which remain important areas of research.

The objective of this study is to describe and quantify how rooftop trees with different crown characteristics influence pollutant removal from urban canyons. By adopting a simplified yet representative urban canyon geometry, the analysis offers new insights into the aerodynamic impact of rooftop trees as green NBS.

The article is structured as follows: Section 2 describes the problem under investigation, discusses and validates the mathematical model, and the computational setup; Section 3 analyses the findings within the urban canyon. The last section summarises the study's conclusions.

2. Problem description and simulation methodology

This study investigates a periodic array of infinitely long three-dimensional urban canyons, with an $AR = 1$. Ambient wind direction is perpendicular to the canyon axis, with a line of trees placed on rooftops. Fig. 1 illustrates the geometric configuration of the urban canyon used in this study. As shown, the pollutant is released from a ground-level line source located at the centre of the street. Nine system configurations are evaluated: one with a smooth roof and eight with trees on rooftops, each featuring a different combination of LAD radial distribution and LAI. The detailed characteristics of these crown morphologies are described in Section 2.7 and summarised in Table 1.

2.1. Case geometry and computational domain

Fig. 1 shows the computational domain, marked by dashed lines, along with an overview of the fully three-dimensional case study geometry, which consists of infinitely repeating urban canyon units. The red region indicates the actual domain simulated. Fig. 1a displays the computational domain used for LES (where the origin of the coordinate system is at the bottom-front corner) marked with dashed line, with dimensions $2H \times 2H \times 3H$ in the streamwise (x), spanwise (y), and vertical (z) directions, respectively.

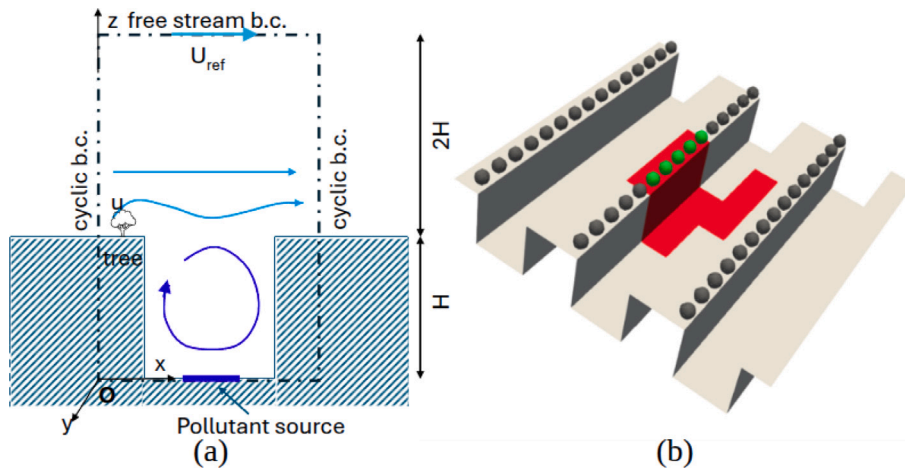


Fig. 1. Panel (a) shows computational domain of urban canyon schematic geometry marked with dotted lines while blue line marks the release of pollutant and O represents origin of the geometry, Panel (b) shows extended section of computational domain of 3D geometry with red region indicating actual domain simulated. (For interpretation of the references to colour in this figure legend, the reader is referred to the web version of this article.)

The trees are placed on the building’s roof at a distance $\delta x = 0.1H$ from the leeward wall, with a diameter of trunk $d = 0.02H$ and a height of trunk $h = 0.15H$. The pollutant concentration (c) is emitted from a ground-level band of width $0.7H$, centred within the street (as depicted by the blue line in Fig. 1a). The source of the pollutant does not span the full canyon width to account for the presence of a footpath.

2.2. Non-dimensional and physical parameters

The Reynolds number based on the free stream velocity and building height is defined as;

$$Re = \frac{U_{Ref} H}{\nu} = 2.0 \times 10^4 \tag{1}$$

where $\nu = 1 \times 10^{-5} \text{ m}^2/\text{s}$ is kinematic viscosity of the fluid (air), H is height of the building and U_{Ref} is the reference velocity. The chosen Reynolds number exceeds the critical value $Re_c = 11,000$, ensuring that the flow is in the Reynolds-independent turbulent regime in the smooth-roof configuration without trees (Chew et al., 2018).

The variables are made non-dimensional by means of characteristic length H , velocity U_{Ref} and time $T = H/U_{Ref}$ of the ambient wind. The characteristic flow time inside of the canyon is $\tau = H/0.1U_{Ref}$. It is observed that the characteristic time of the vortex inside the canyon is obtained by considering an empirical estimate of the characteristic velocity equal to $0.1U_{Ref}$ (Cintolesi et al., 2021). The pollutant flow rate at the source is defined as $q = \lambda \partial c / \partial n$, where λ is the molecular diffusivity and n is the surface-normal direction. The reference concentration is $C_{Ref} = q/U_{Ref}$, which is used to normalise the concentration values.

2.3. Mathematical models

The flow dynamics is described by the incompressible Navier–Stokes equations:

$$\frac{\partial u_i}{\partial x_i} = 0 \tag{2}$$

$$\frac{\partial u_i}{\partial t} + u_j \frac{\partial u_i}{\partial x_j} = -\frac{1}{\rho_0} \frac{\partial p}{\partial x_i} + \nu \frac{\partial^2 u_i}{\partial x_j \partial x_j} + S_{u,i} \tag{3}$$

where u_i are the velocity components, x_i are the Cartesian coordinate, t is time, ρ_0 is the reference density, p is the pressure, ν is the kinematic viscosity and $S_{u,i}$ is the sink term momentum equation that model the tree crown.

The tree crown is modelled as porous media in analogy with the model used for forest canopy (Cintolesi et al., 2023). The elements that compose the tree crown (like foliage, leaves, and branches) cause a loss (sink) of momentum. The crown is here modelled as a sphere with a variable density from the centre to the boundaries. Such a variation of density is described by a radial LAD profile. The sink term for the momentum equation is (Dalpé and Masson, 2009):

$$S_{u,i} = -C_d \alpha |u| u_i \tag{4}$$

where C_d is the drag coefficient of the tree canopy and α is the crown radial LAD. Pollutant emission due to traffic is modelled as a passive scalar and the concentration term is described by:

$$\frac{\partial c}{\partial t} + u_i \frac{\partial c}{\partial x_i} = \lambda \frac{\partial^2 c}{\partial x_i \partial x_i} \quad (5)$$

where λ is molecular diffusivity and c is concentration.

2.4. Numerical approach and setup

In the context of LES, the computational grid imposes an implicit spatial filter on the governing equations (Sagaut, 2005; Rodi et al., 2013). The filtering of the equations introduces additional terms accounting for unresolved subgrid scales of motion, represented by the SGS kinematic momentum and mass fluxes.

The overbar denotes the spatial filter of width equal to the computational cell size, estimated as $\bar{\Delta} = (\Delta_x \Delta_y \Delta_z)^{1/3}$. The SGS kinematic momentum fluxes are expressed by means of the Smagorinsky model (Smagorinsky, 1963):

$$\tau_{ij} - \frac{\delta_{ij}}{3} \tau_{kk} = -2\nu_{SGS} \overline{S_{ij}}, \quad (6)$$

where $\nu_{SGS} = c_s^2 \bar{\Delta}^2 |\overline{S_{ij}}|$ is the SGS viscosity, $S_{ij} = (1/2)[(\partial \bar{u}_i / \partial x_j) + (\partial \bar{u}_j / \partial x_i)]$ is the resolved strain rate tensor, $|\overline{S}| = (2\overline{S_{ij}}\overline{S_{ij}})^{1/2}$ is its magnitude, c_s is the Smagorinsky constant. For the closure of the concentration equation, Reynolds' analogy is adopted for the SGS diffusivity:

$$h_i = -\lambda_{SGS} \frac{\partial \bar{c}}{\partial x_i} \quad (7)$$

where $\lambda_{SGS} = \nu_{SGS} / Sc_t$, and $Sc_t = 0.85$ is the turbulent Schmidt number. Additional details and methodologies related to the SGS model employed in this study are based on the framework outlined by Cintolesi et al. (2015). The tree model adopted in this study, based on porous medium formulation, has been previously validated against both LES and RANS using wind tunnel measurements in the study by Poh et al. confirming its capability to realistically represent the aerodynamic behaviour of vegetation canopies (Poh et al., 2020).

Numerical simulation is performed using the open-source code OpenFOAM (version 6.0) (The OpenFOAM Foundation, 2018), modifying the original solver pimpleFoam to include transport equations for pollutant concentration. For temporal discretisation, an implicit Euler backward scheme is employed, while a second-order central difference scheme is used for spatial discretisation, except for the concentration advective term. The Gauss-Gamma scheme ($\gamma = 0.2$), proposed by Jasak et al. (1999), is applied for this term. To avoid non-physical negative concentration values that could arise in a few cells at the street level during flow development, a numerical clipping procedure is applied. Overall, the numerical accuracy is of second-order.

2.5. Computational mesh and boundary conditions

The computational domain is discretised using a structured mesh, with finer resolution applied in regions of high gradient, such as near solid boundaries and within the vegetation region. To accurately capture the flow-vegetation interactions, the mesh is locally refined in a rectangular section surrounding the porous tree volume, allowing for better resolution of momentum sink effects introduced by the vegetation model. The computational mesh for the smooth-roof case consists of 1,764,902 computational cells with $y^+ < 1$ at the binding surfaces to ensure a direct resolution of the wall-boundary layer, and a refinement at the roof level ($z/H = 1$) where high levels of turbulence are localised. The tree cases are discretised by 2,294,706 cells, with $y^+ < 1.5$. Fig. A.17 visually shows the mesh structures.

The boundary conditions are as follows: cyclic boundary conditions to vertical sides for all variables in order to simulate an infinite extension in both the streamwise and spanwise directions. The airflow is defined by a freestream velocity (U_{Ref}), representing the average streamwise velocity at the top boundary of the computational domain. At the solid boundaries, a no-slip condition is imposed for velocity, while a zero-gradient for pressure and concentration. At the domain upper boundary, a zero-gradient condition is applied to velocity, while pressure and concentration are set to zero. An imposed body force drives the fluid; this is dynamically computed to guarantee that the average velocity at the top face of the domain is $U_{Ref} = 0.2$ m/s. The simulation is initialised with a uniform velocity field of $u_x = 0.2$ m/s. The time step is dynamically adjusted to maintain a Courant–Friedrichs–Lewy (CFL) number below 0.5, which is a common recommendation in LES to ensure numerical stability. After reaching a steady-state condition, the simulation is run for an additional 12τ . To ensure statistical convergence, particularly in the presence of rooftop trees, 600 instantaneous fields are saved at uniform intervals throughout the 12τ time window. Statistics are calculated over time and along the spanwise direction. A posteriori analysis confirmed that the sampling and the time window chosen are sufficient to achieve stable statistics.

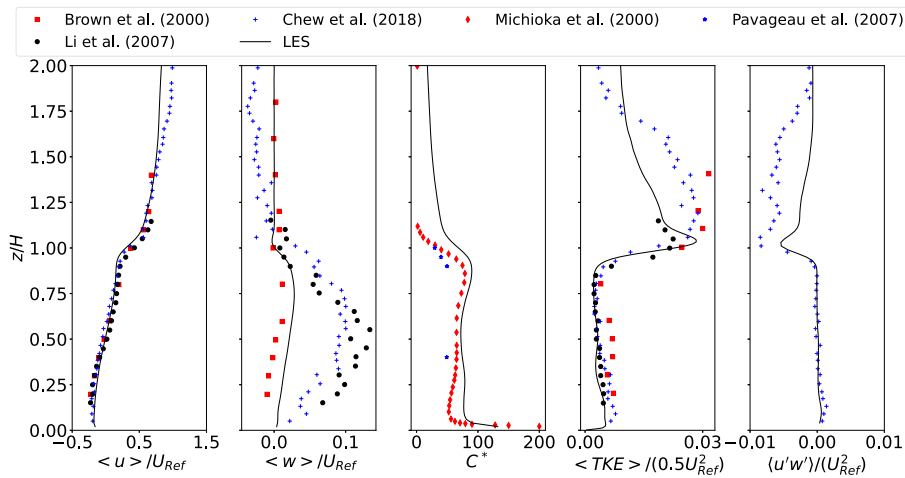


Fig. 2. Comparison of simulation results against datasets of Brown et al. (2000), Li et al. (2008), Chew et al. (2018), Pavageau and Schatzmann (1999), and Michioka et al. (2011). From left to right, non-dimensional mean horizontal velocity ($\langle u \rangle / U_{Ref}$), vertical velocity ($\langle w \rangle / U_{Ref}$), concentration (C^*), TKE ($\langle TKE \rangle / (0.5U_{Ref}^2)$), and resolved kinematic momentum flux ($\langle u'w' \rangle / (U_{Ref}^2)$) along the vertical line $x/H = 1.00$.

2.6. Validation summary

The validation of the baseline case (no rooftop trees) has been carried out and extensively discussed in a previous work by Cintolesi et al. (2021), comparing simulation results with against existing numerical and laboratory datasets of Brown et al. (2000), Li et al. (2008), and Chew et al. (2018) while concentration profile is validated against datasets from Meroney et al. (1996), Pavageau and Schatzmann (1999), and Michioka et al. (2011). For the sake of conciseness, the full validation has not been repeated, but a short discussion on selected variables is reported here for completeness.

Fig. 2 shows a selection of first- and second-order statistics, made non-dimensional and averaged in time and spanwise direction. The streamwise velocity profile exhibits excellent agreement with the experimental datasets. The vertical velocity shows some discrepancies inside the canyon compared to the dataset of Li et al. (2008) and Chew et al. (2018), however it shows good agreement with the data set of Brown et al. (2000). This behaviour is consistent with the findings reported in Cintolesi et al. (2021), in which this deviation in vertical velocity is well documented. The concentration profile matches the laboratory experiment of Michioka et al. (2011). The reference profiles in the external region rapidly decrease to zero as a result of the pollution being enclosed within a single canyon and the presence of clear fluid flowing above it. The LES profile assumes non-zero values that decline gradually with height as a result of the pollutant removal from the canyons. This trend can be attributed to the transport and removal of pollutants from canyons. The turbulent kinetic energy (TKE) and the resolved kinematic momentum flux profiles exhibit a good agreement with the benchmark dataset within the canyon ($x/H < 1.00$) and reproduce the benchmark results of Li et al. (2008) in the external region. The LES results underestimate the momentum flux profiles outside the canyon ($x/H > 1.00$) when compared to the findings of Chew et al. (2018). Minor discrepancies observed at specific locations are noted; however, they do not substantially affect the overall validity of the findings. The limited streamwise domain size ($2H$) may constrain the development of large-scale eddies above the canyon, as discussed by Michioka et al. (2011). However, they do not critically affect the mass and momentum exchange at the canyon-atmosphere interface. Overall, the LES approach effectively captures the primary flow dynamics within the domain. The domain height ($3H$) is verified to be sufficient, as vertical profiles indicate convergence near the top boundary across all cases, showing negligible variation near the top boundary and, thus, indicating minimal influence from not resolved higher-layer structures. Prior studies suggest that while outer-scale eddies may affect pollutant removal in open environments, their impact on pollutant dispersion from urban canyons is less significant in quasi-steady cross-canyon flows, especially in geometries with $AR = 1$ (Michioka et al., 2011). Hence, the domain height is considered satisfactory for the aim of the present study. To further assess the accuracy of the simulation, the LES Index of Quality (LESIQ) is computed following the formulation proposed by Qin et al. (2024). The averaged values are $LESIQ = 0.9$, that is above the threshold of 0.8 proposed by Pope (2001). Thus, this indicates that the simulation resolves a substantial portion of the turbulence energy.

The tree crowns in this study are modelled using a porous-medium approach based on radial LAD distribution. A direct validation of the model used for trees has not been carried out since the porous-medium formulation adopted here has been extensively validated in prior literature. For instance, Poh et al. (2020) demonstrated excellent agreement of LES and RANS models with wind tunnel data. Additional studies by Endalew et al. (2009), Kang et al. (2020), and Xu et al. (2022) have validated the porous-medium model for trees using RANS against wind tunnel and field measurements. These previous works support the suitability of the porous-medium model for tree representation employed here.

Table 1
Simulation cases by tree characteristics: LAI and LAD distributions.

LAI	LAD			
	Dense	Linear	Power	Constant
8	DLAI8	LLAI8	PLAI8	CPLAI8
11	DLAI11	LLAI11	PLAI11	CPLAI11

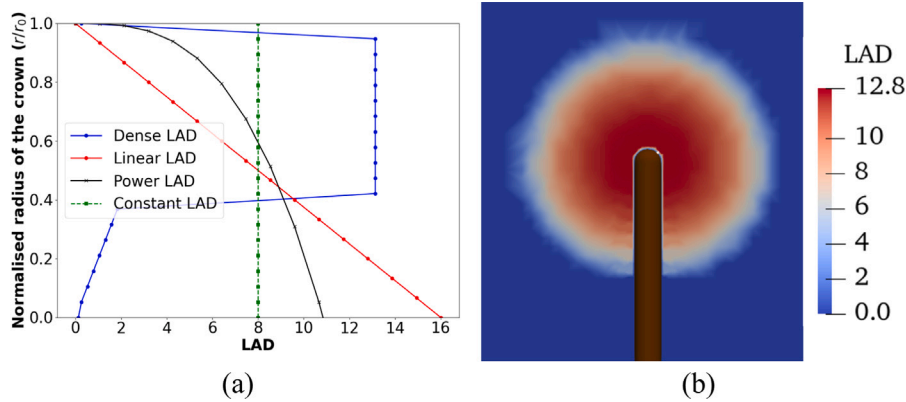


Fig. 3. Panel (a): Radial Leaf Area Density (LAD) profiles for a tree crown with $LAI = 8$, illustrating Dense, Linear, Power, and Constant distributions. Panel (b): Contour plot for ($PLAI8$), highlighting radial foliage distribution around the crown.

2.7. Tree morphology description

The tree morphology in this study is characterised by four parameters: the crown drag coefficient (C_d), the radius of the crown (r_0), the LAI, and the crown radial LAD. The LAI is defined as the integral of LAD across the crown height. The C_d can vary between 0.1 and 0.3 for vegetated elements, while for tree crown, the common value of $C_d = 0.2$ is usually utilised (Katul and Albertson, 1998; Marcolla et al., 2003; Pinard, 2002). A constant value of C_d is adopted in this study, consistent with prior literature that demonstrated this value as a representative average for tree-like vegetation, especially in porous media models (Katul and Albertson, 1998; Gromke and Blocken, 2015a). It is worth noticing that recent studies have pointed out that a more realistic representation of the tree crown would require higher values of the drag coefficient, which is estimated in the range $0.5 < C_d < 0.9$ after the most recent wind tunnel and real field experiment (Zeng et al., 2020). In the present study, the classical values $C_d = 0.2$ in accordance with existing literature. The radius of the crown is set to $r_0 = 0.1/H$ to ensure a practical tree size for rooftop placement. A larger radius would make the tree unsuitable for a rooftop, while a smaller radius would result in minimal impact on airflow and pollutant dispersion. Regarding the LAI and LAD, we use different values of these parameters to conduct a parametric study. The LAI values adopted in this study (8 and 11) are selected as high and very high values of LAI to perform the parametric study and to evaluate the limiting aerodynamic influence of rooftop vegetation (Jiménez et al., 1996). It is worth noticing that such values can be suitable for modelling dense forest canopies and may exceed typical ranges observed in rooftop vegetation (Moser-Reischl et al., 2025). The crown morphology is represented as a sphere since a large part of tree crowns can be approximated as a spherical form. LAI values of 8 and 11 represent dense foliage and serve as upper-bound parameters. As the influence on canyon flow and dispersion is already minimal, lower LAI values typical of rooftop vegetation (2–5) are expected to be negligible. Future studies should examine non-spherical crowns and moderate LAI ranges. Nevertheless, $LAI = 8$ is a realistic value for some plant species with particularly dense foliage that can be found in urban environments; e.g. *buxus sempervirens*, *euonymus japonicus*, *figus benjamina* (Neinavaz et al., 2016). Four different profiles are chosen for the crown radial LAD: Dense profile ($DLAI8$) has a low LAD near the canopy centre, which increases outward to a specific radius and then remains constant to the outer radius; the Linear profile ($LLAI8$) exhibits a linear decrease in LAD with increasing radial distance from the canopy centre and its formula is $LAD = -15(r/r_0) + 16$, where $r/r_0 \in [0, 1]$; the Power profile ($PLAI8$) follows a nonlinear decrease, representing a polynomial distribution where LAD diminishes more rapidly as it moves outward, while the formula is $LAD = [1280 - 1280(r/r_0)]^{1/3}$; the Constant Profile ($CPLAI8$) maintains a uniform LAD from the canopy centre to the outer radius. The four profiles are shown in Fig. 3, while the summary of the eight simulations performed with trees is reported in Table 1.

3. Results

3.1. Flow dynamics in the urban canyon

To analyse the flow and scalar transport dynamics, the computational domain is divided into four vertical layers based on normalised height z/H : the pedestrian layer ($0 = z/H < 0.15$), the middle layer ($0.15 < z/H < 0.85$), the mixing interface

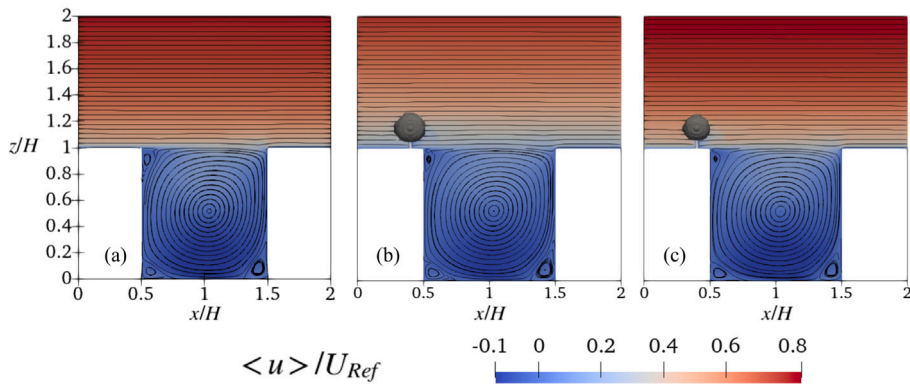


Fig. 4. Streamlines and distribution of horizontal velocity averaged in time and spanwise direction for (a) smooth-roof case, (b) DLAI8, and (c) PLAI8.

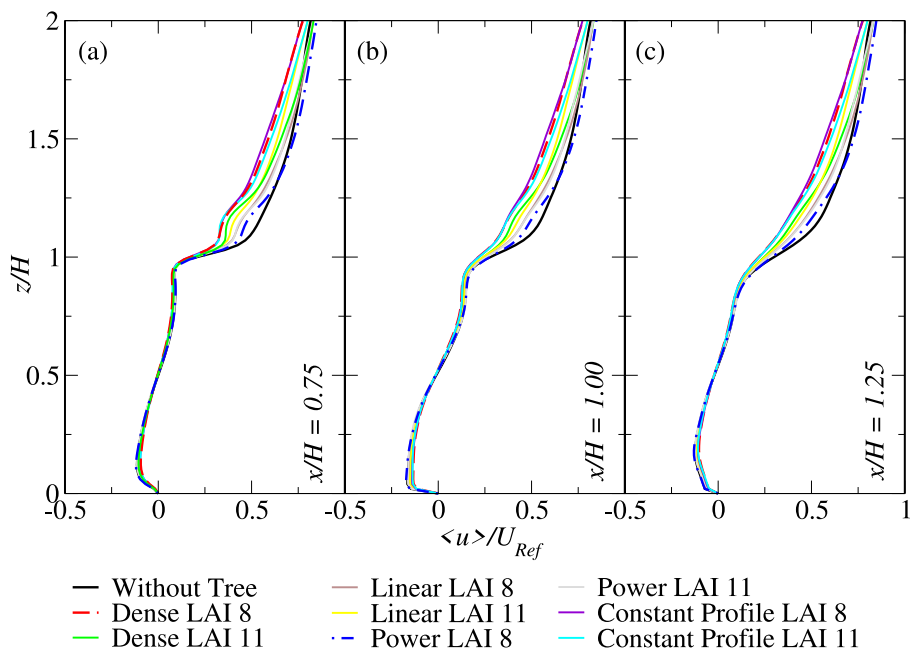


Fig. 5. Non-dimensional horizontal velocity component profiles averaged in time and spanwise direction at three locations: $x/H = 0.75, 1.00, 1.25$ for panel (a), (b) and (c), respectively.

($0.85 < z/H < 1.25$), and the outer layer ($z/H > 1.25$). These layers are selected to correspond with the street-level region most affected by pollutant release, the core canyon vortex zone, the mixing layer at rooftop level, and the flow region above the canyon, respectively.

Fig. 4 shows the streamlines of the non-dimensional horizontal velocity averaged in time and spanwise direction for the smooth-roof case and for the case of DLAI8 and PLAI8. The canyon features a primary vortex at the centre and three stable low-velocity circulation zones located at its corners. The height of the primary vortex is maximum at the height of the interface between the vortex and the ambient flow. Fig. 4(b), (c) show a low-velocity zone at the bottom of the tree due to the trunk acting as a solid medium. Line profiles are extracted at $x/H = 0.75, 1.0,$ and 1.25 , corresponding to locations near the centre of the canyon at the windward and leeward facades, respectively, from within the canyon: $y/H = 0.0-2.00$. Line profiles for all of the cases are presented in Fig. 5 at three locations: $x/H = 0.75, 1.00, 1.25$ for panels (a), (b) and (c), respectively, and it shows minimal variation in the pedestrian and middle layer. The horizontal velocity in the mixing interface reduces for the case of trees, as the crown acts as a porous medium. The case of DLAI8, CPLAI8, and CPLAI11 has dense foliage in the outer layer of its crown, therefore, it shows low horizontal velocity in the mixing interface. The case of PLAI8 has a low density of foliage in the outer layer of its crown, thereby it almost overlaps with the case without trees. Trees do not affect the sharp separation of horizontal velocity created at the rooftop. In general, trees do not significantly impact the behaviour of the flow within the canyon, as the contour plot and line

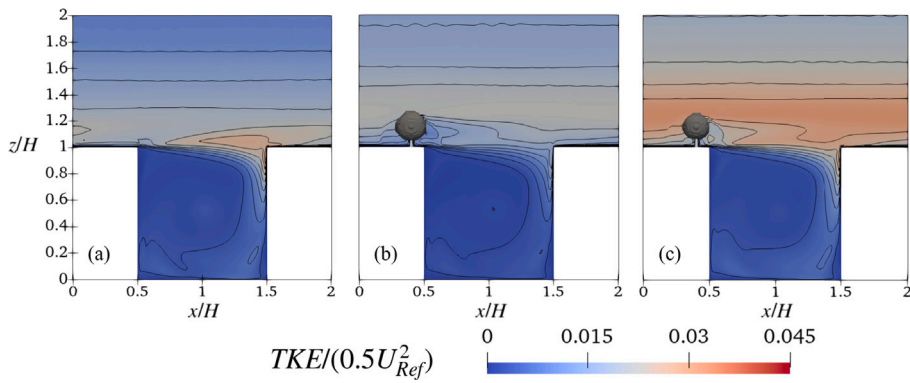


Fig. 6. Non-dimensional contour plot of TKE averaged in time and spanwise direction for (a) smooth-roof case, (b) DLAI8, and (c) PLAI8.

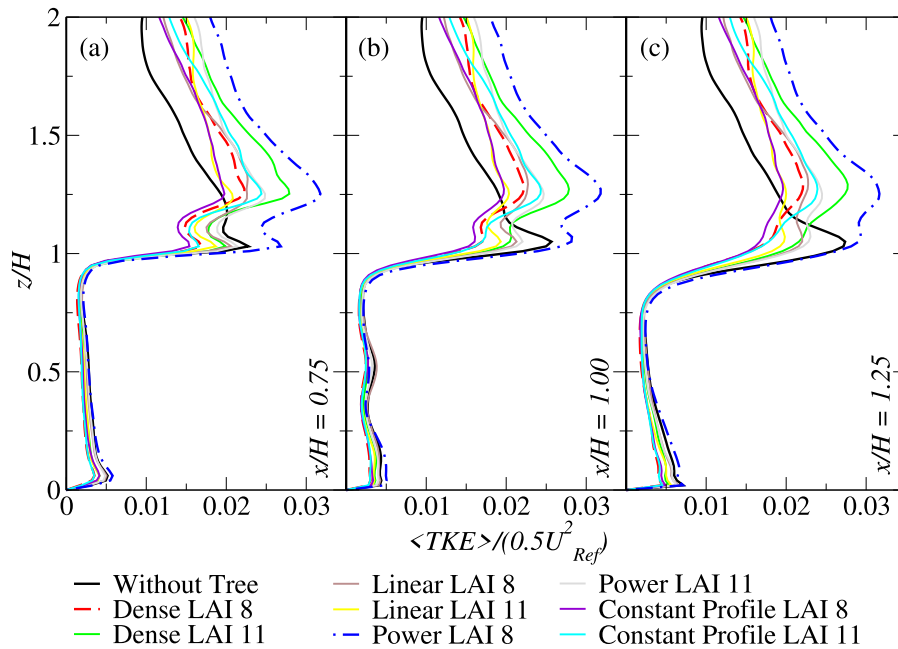


Fig. 7. Non-dimensional TKE profile averaged in time and spanwise direction at three locations: $x/H = 0.75, 1.00, 1.25$ for panel (a), (b), and (c) respectively.

profiles show similar behaviour of the horizontal velocity within the canyon. The vertical velocity component exhibits no significant differences; therefore, it is not discussed here.

Fig. 6 presents the contour plot of non-dimensional TKE averaged in time and spanwise direction for the smooth-roof case and the case with trees (*DLAI8* and *PLAI8*). TKE exhibits similar behaviour within the canyon for the smooth-roof case and for the case with trees. For *DLAI8*, horizontal velocity is reduced at the mixing layer as can be seen in Fig. 5 due to dense foliage in the outer layer of the crown, resulting in higher TKE in the outer layer as compared with the smooth-roof case. Conversely, for *PLAI8*, the higher shear term is due to compact foliage in the centre of the crown and therefore, higher TKE is observed at the mixing interface and in the outer layer. Fig. 7 shows line profiles for the case of trees and the smooth-roof case at three locations: $x/H = 0.75, 1.00, 1.25$ for panels (a), (b) and (c), respectively. In the pedestrian and middle layers, the TKE exhibits similar behaviour across all cases, with *PLAI8* showing a slightly higher TKE value compared to the other cases. The presence of a tree disrupts the airflow on the rooftop. For the smooth-roof case, there is one local maximum at the rooftop due to the shear layer of the roof, while for the case of trees, there are two local maxima at the rooftop due to the shear layer produced by the trees and the rooftop. The case of *DLAI8* and *CPLAI8* presents lower TKE from $1.2 < z/H < 1.6$ as compared with the other cases due to dense foliage around its corners. Trees introduce complexity to the flow field by disrupting the uniformity of the flow in the mixing and outer layers. Extreme cases for the trees are discussed as the remaining cases lie between them. Based on the analysis of horizontal velocity and TKE, the eight cases exhibit intermediate velocity profiles between the cases of *DLAI8* and *PLAI8*. Due to this reason, the cases of smooth-roof, *DLAI8*, and *PLAI8* have been selected as the most interesting cases and analysed in depth.

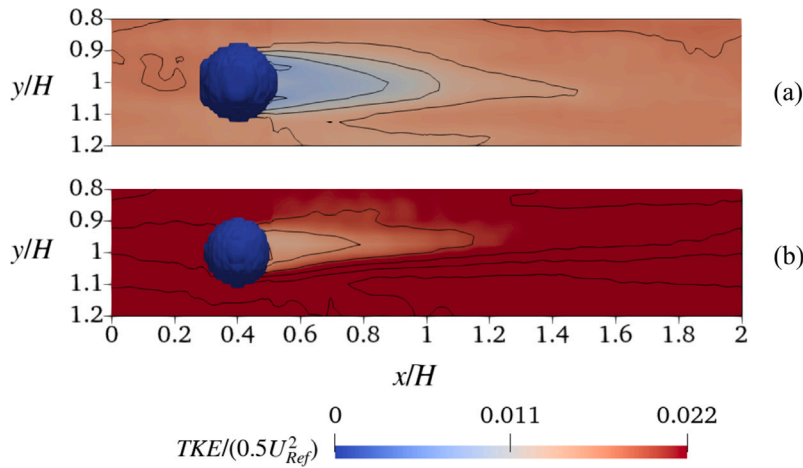


Fig. 8. Contour plot of non-dimensional TKE averaged in time and spanwise direction at the horizontal plane $z/H = 1.15$: for (a) DLAI8, and (b) PLAI8.

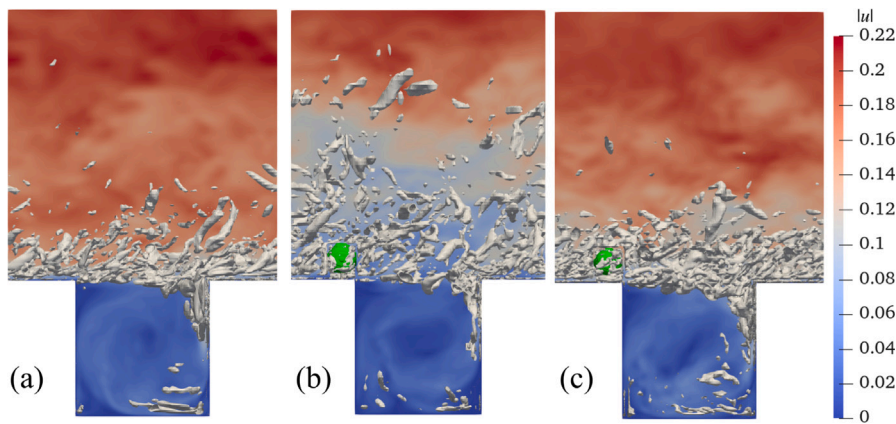


Fig. 9. Turbulent structures visualised by the isosurface of scalar Q , together with the instantaneous velocity magnitude at a vertical slice in the background at $y/H = 1.00$: for (a) smooth-roof case, (b) DLAI8, and (c) PLAI8.

Fig. 8 shows a contour plot of non-dimensionalised TKE averaged in time and spanwise direction at the horizontal plane $z/H = 1.15$, for the cases of *DLAI8* and *PLAI8*. In both cases, low TKE values are observed immediately downstream of the crown, where the porous foliage dampens turbulent fluctuations. However, the overall TKE magnitude is significantly higher in the *PLAI8* case. This can be attributed to the crown morphology: *PLAI8* has a more compact core and lower foliage in the outer region, which promotes the development of stronger velocity shear around the crown boundary and enhances turbulence generation. In contrast, *DLAI8* has denser foliage distributed near the outer canopy, which smooths shear gradients and results in more uniformly dampened turbulence.

Instantaneous coherent turbulent structures are visualised using the Q -criterion, following the method of [Dubief and Delcayre \(2000\)](#), which identifies vortical regions where rotation dominates over strain. **Fig. 9** presents a visual comparison of these structures for three scenarios, highlighting how the presence and morphology of rooftop trees affect the spatial distribution and intensity of turbulence. In the smooth-roof case, turbulent structures are concentrated within the mixing layer and near the downwind façade of the building. In the *PLAI8* case, the crown is compact and centred, allowing flow to pass more freely above and around the tree. This generates shear near the crown boundary, producing coherent vortices that remain largely confined within the mixing layer ($1.0 < z/H < 1.5$). In contrast, the *DLAI8* crown has higher LAD near the canopy edges, acting as a more effective aerodynamic barrier. This slows down the flow more significantly and enhances vertical momentum transport. As a result, turbulence is transported and vortical structures are observed extending into the upper part of the domain. Although the overall TKE is lower for *DLAI8*, the structure and spatial distribution of turbulence are strongly influenced by crown morphology. This interpretation is consistent with the TKE patterns shown in **Fig. 8**, highlighting the importance of LAD distribution in modulating rooftop airflow.

Fig. 10 presents the contour plot of turbulent kinematic momentum flux for the cases of trees (*DLAI8* and *PLAI8*) and the smooth-roof case. For the smooth-roof case, the turbulent kinematic momentum flux is higher in the pedestrian and middle layers

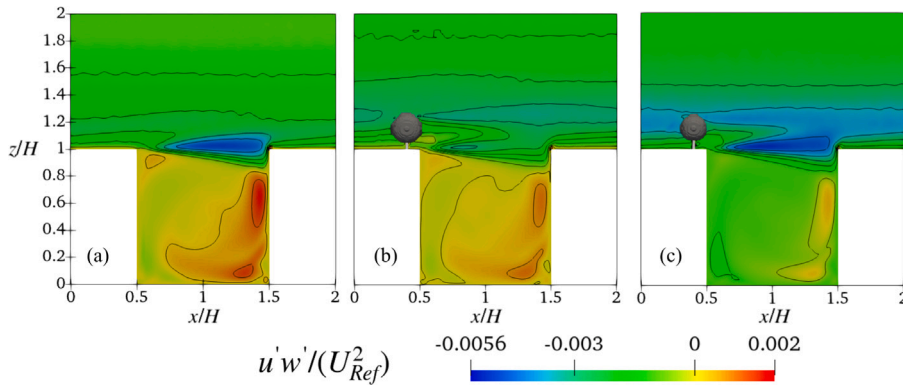


Fig. 10. Contour plot of non-dimensional turbulent kinematic momentum flux ($\langle u'w' \rangle / U_{Ref}^2$) averaged in time and spanwise direction for (a) smooth-roof case, (b) DLAI8, and (c) PLAI8.

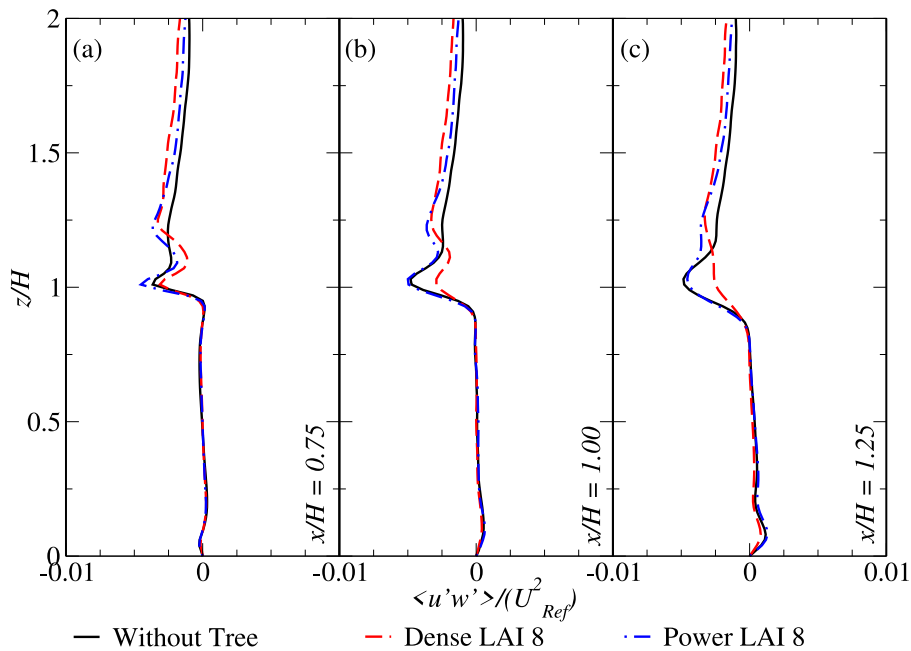


Fig. 11. Non-dimensional turbulent kinematic momentum flux ($\langle u'w' \rangle / U_{Ref}^2$) profiles averaged in time and spanwise direction at three locations: $x/H = 0.75, 1.00, 1.25$ for panels (a), (b) and (c), respectively.

of the downwind facade, indicating downward momentum transfer. In contrast, the presence of trees reduces the turbulent kinematic momentum flux at the pedestrian and middle layer. At the mixing interface, smooth-roof and PLAI8 exhibit vertical momentum transfer in an upward direction at the rooftop due to the shear layer of the wind. Fig. 11 illustrates the line profiles of turbulent kinematic momentum flux at three locations: $x/H = 0.75, 1.00, 1.25$ for panels (a), (b) and (c), respectively. The results show similar behaviour within the pedestrian and middle layer for all of the cases. At the mixing interface for the smooth-roof case, it reveals one local maximum, while for the case of trees, it indicates two local maxima. The top-upwind circulation zone in Fig. 4 is created by a sharp and highly energetic shear layer at the rooftop, as shown in Fig. 11 near $z/H = 1.00$. Fig. 6 indicates higher TKE for the smooth-roof case as compared with the case of DLAI8 at the mixing layer near the downwind facade due to the shear layer at the rooftop. In the outer layer, turbulent kinematic momentum flux shows approximately similar behaviour for the smooth-roof and the case of trees, as can be seen from Figs. 10, 11.

3.2. Concentration behaviour in the urban canyon

Fig. 12 displays the contour plot of the non-dimensionalised logarithm of concentration for the cases of trees (DLAI8 and PLAI8) and the smooth-roof case. A high concentration is observed at the bottom of the canyon within the pedestrian layer due to the direct

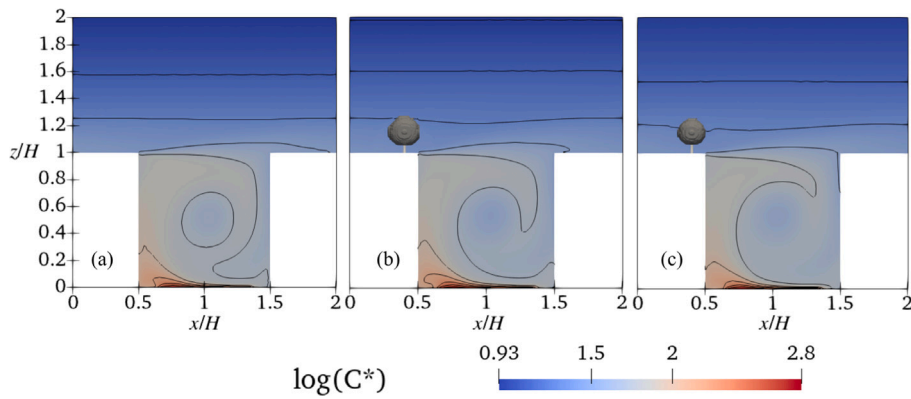


Fig. 12. Contour plot of non-dimensional concentration log averaged in time and spanwise direction for (a) smooth-roof case, (b) DLAI8, and (c) PLAI8.

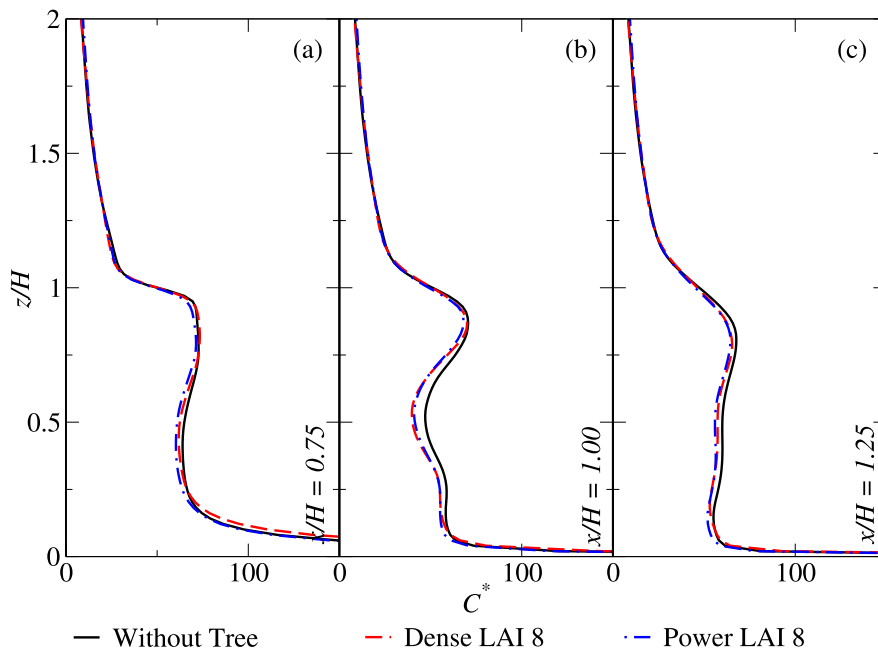


Fig. 13. Non-dimensional time-averaged concentration profile averaged in time and spanwise direction at three locations: $x/H = 0.75, 1.00, 1.25$ for panels (a), (b) and (c), respectively.

release of concentration from the street. The middle layer and mixing interface show a decrease in concentration due to interactions between the canyon and the surrounding environment. Fig. 13 presents non-dimensionalised concentration profiles at three locations: $x/H = 0.75, 1.00,$ and 1.25 for panels (a), (b) and (c), respectively. At all locations, the highest concentration is observed in the pedestrian layer, where pollutant removal is released. The middle layer shows an intermediate amount of concentration, while the mixing interface shows lower concentration levels, consistent with improved turbulent mixing at the rooftop level. At $x/H = 1.00$ and 1.25 , both *DLAI8* and *PLAI8* cases show lower concentrations in the middle layer compared to the smooth-roof case. In contrast, at $x/H = 0.75$, which is closer to the canyon inlet, the line profiles across all three configurations overlap closely, indicating that tree effects on dispersion are less pronounced near the inflow. In the outer layer ($z/H > 1.25$), all cases converge to similar concentration levels, suggesting that rooftop vegetation does not significantly alter the pollutant removal efficiency at the outer layer. In general, the amount of concentration removal remains the same for the case of trees and the smooth-roof case.

Fig. 14 reports the profiles of horizontal turbulent concentration flux at three locations: $x/H = 0.75, 1.00, 1.25$ for panels (a), (b) and (c), respectively. In the pedestrian layer, a higher concentration is observed, consistent with the contour plot of concentration (see Fig. 12), as the pollutant is released from the bottom of the canyon. The line profiles exhibit similar behaviour in the middle layer, while a local maximum with a negative value appears at the mixing interface, due to the shear layer at the rooftop.

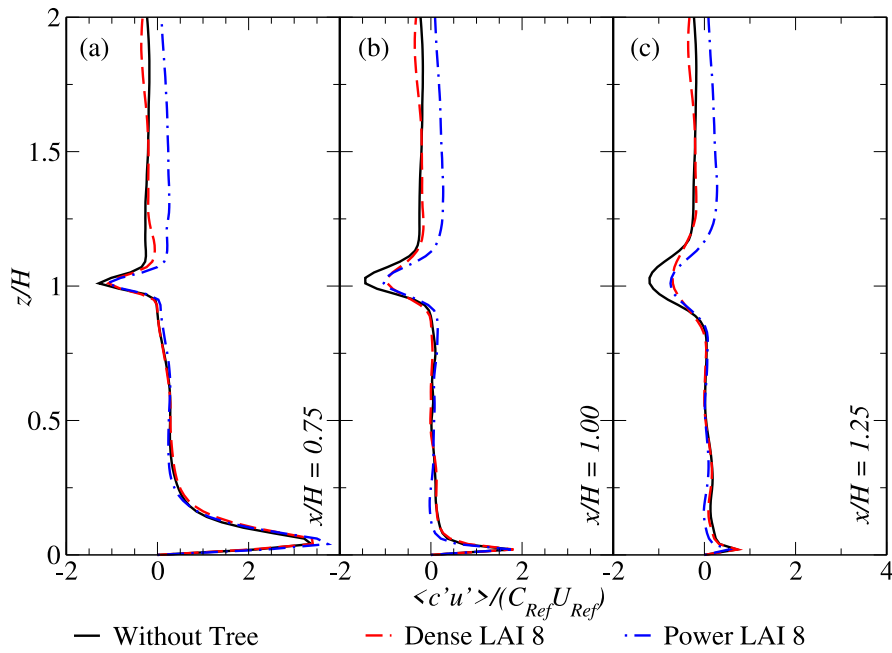


Fig. 14. Non-dimensional horizontal turbulent concentration flux ($\langle c'u' \rangle / C_{Ref} U_{Ref}$) profile averaged in time and spanwise direction at three locations: $x/H = 0.75, 1.00, 1.25$ for panels (a), (b) and (c), respectively.

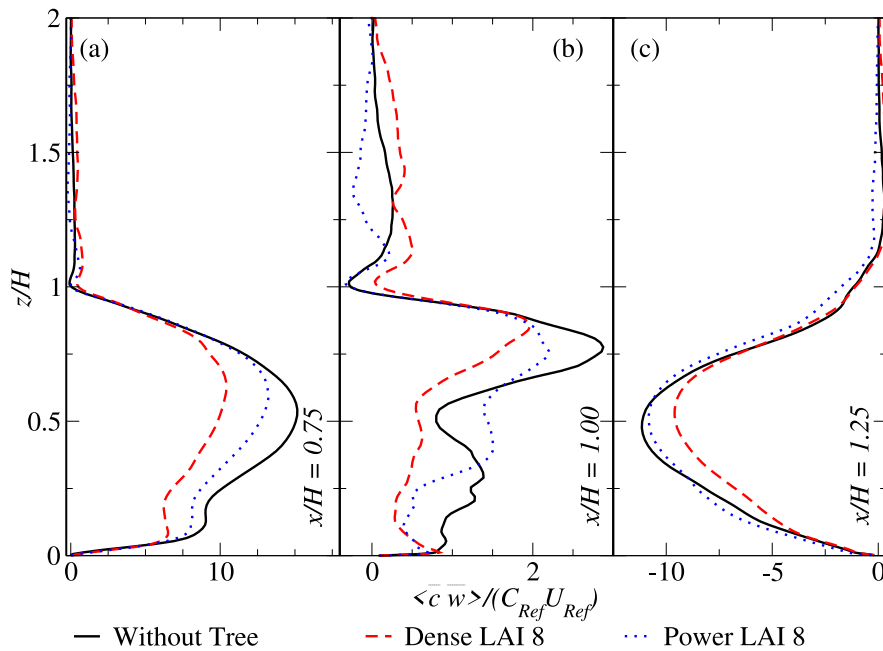


Fig. 15. Line profiles of convective scalar flux ($\langle \bar{c} \bar{w} \rangle / C_{Ref} * U_{Ref}$) for the smooth-roof case, *DLAI8*, and *PLAI8* configuration at three locations: $x/H = 0.75, 1.00, 1.25$ for panel (a), (b) and (c), respectively.

Fig. 15 illustrates line profiles of mean vertical concentration flux for the smooth-roof case and for the case of trees at three locations: $x/H = 0.75, 1.00, 1.25$ for panels (a), (b) and (c), respectively. A higher amount of mean concentration flux is observed within the canyon at all three locations, while the smooth-roof case shows a higher amount of concentration flux as compared with the case of trees. The amount of mean concentration flux outside of the canyon is similar for the smooth-roof case with the case of trees at all three locations.

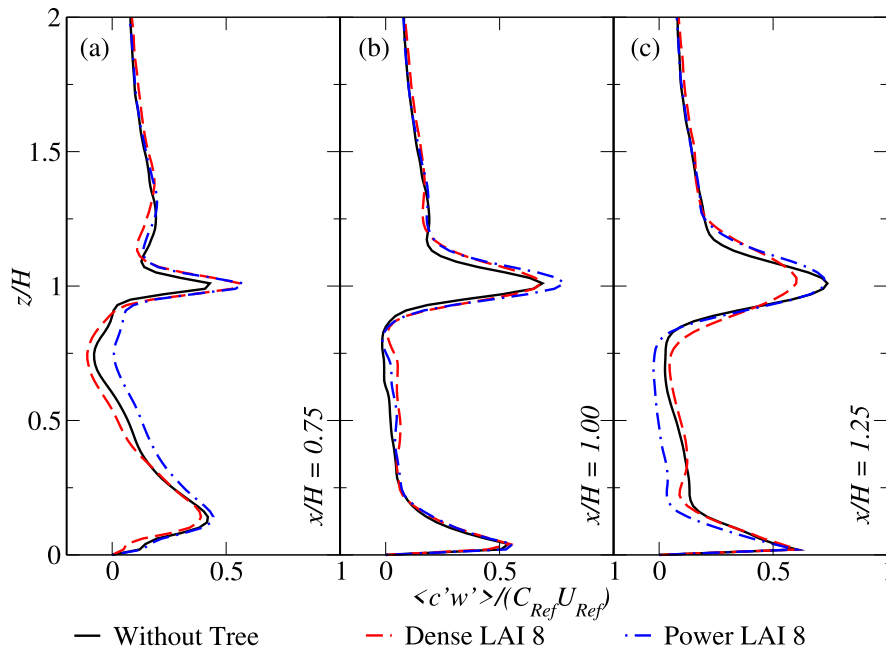


Fig. 16. Non-dimensional vertical turbulent concentration flux ($\langle c'w' \rangle / C_{Ref} U_{Ref}$) profile averaged in time and spanwise direction at three locations: $x/H = 0.75, 1.00, 1.25$ for panel (a), (b) and (c), respectively.

Fig. 16 shows profiles of vertical turbulent concentration flux for the smooth-roof case and for the case of trees at three locations: $x/H = 0.75, 1.00, 1.25$ for panels (a), (b) and (c), respectively. Higher vertical turbulent concentration flux is observed in the pedestrian layer, while the middle layer exhibits less pronounced differences. A local maximum is observed at the rooftop within the mixing interface, whereas the outer layer shows a limited difference.

4. Conclusion

This study evaluates how rooftop trees, as a green NBS, affect pollutant dispersion in a square urban canyon. A simplified configuration is numerically reproduced using Large-Eddy Simulation (LES), where the tree crowns are modelled as porous media. Nine different configurations of the system are reproduced: the baseline without trees in the building roof, and eight cases with rooftop trees having different crown characteristics, obtained by varying leaf radial distribution (radial LAD) and density index (LAI).

Overall, the presence of rooftop trees mainly affects the out-canyon flow (mean velocity, turbulent kinetic energy, and turbulent kinematic flux), while the in-canyon dynamics remain substantially unaltered. The addition of rooftop trees marginally affects the mixing interface between the canyon and the atmosphere, hence, this does not help improve the removal of pollutants from the canyon. This result is unexpected to some extent: intuition may suggest that the presence of rooftop trees would reduce the atmospheric wind speed, and thus would lead to a reduction in the ventilation of the canyon. Overall, rooftop trees have a minimal impact on in-canyon pollutant concentration, and the resulting concentration distribution is essentially unchanged compared to the smooth-roof case.

Regarding the differences among the crowns investigated, it is found that the radial LAD is the key parameter determining the impact of trees on the system. The crown where the leaf distribution is higher on the outer edge (e.g. case *DLAI8*) generates a uniform and effective barrier (momentum sink) to the ambient wind, which reduces the averaged wind velocity and turbulent kinetic energy. The crown that has a more compact leaf density distribution (concentrated on the centre, e.g. case *PLAI8*) behaves as an isolated obstacle, not substantially altering the wind speed (except at tree level) and triggering high TKE values.

From an application perspective, the study suggests that the use of trees on roofs is a solution to increase urban vegetation with related co-benefits (e.g. shading of streets or pollutant deposition) without negatively impacting the dispersion of pollutants in the canyon, which is a typical side effect of street-level vegetation that can reduce ventilation and increase pollutant concentration within urban canyons. Several simplification assumptions are adopted, including geometrical (spherical tree crowns, square canyon, infinite array of canyons) and dynamical (low Reynolds number) assumptions. Although the simplified case does not reproduce the full complexity of real urban environments, it represents a typical case widely used in the literature. The use of a simplified configuration allows the isolation and identification of the dominant mechanisms governing airflow and pollutant dispersion in the presence of rooftop trees.

These can support the integration of rooftop trees as effective Nature-Based Solutions (NBS) within urban planning frameworks.

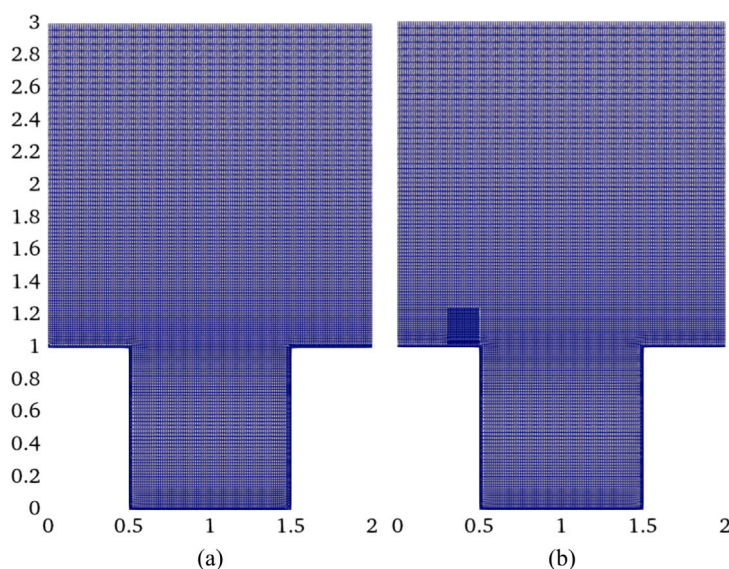


Fig. A.17. Computational mesh used in LES simulations: (a) smooth-roof case, (b) tree case with locally refined mesh around the porous tree volume to capture vegetation-flow interaction.

This study employed simplified assumptions (e.g., spherical crowns, high LAI values, absence of thermal and seasonal effects) to isolate aerodynamic mechanisms. While such a choice enables a focused parametric investigation and reproduces cases where the ambient wind is the predominant dynamical force, future studies should extend this framework by also incorporating thermal processes. Real rooftop vegetation often has irregular geometries, lower LAI, and seasonal variability (e.g., defoliation, phenological changes) that affect pollutant deposition and wind interaction. Future research should integrate moderate LAI scenarios, diverse morphologies, seasonal factors, and complex urban geometries to enhance direct applicability for city planners.

CRediT authorship contribution statement

Malik Safi Ullah: Writing – original draft, Visualization, Validation, Software, Methodology, Investigation, Formal analysis, Data curation, Conceptualization. **Alessandro Di Giulio:** Software, Methodology. **Carlo Cintolesi:** Writing – review & editing, Supervision, Resources, Methodology, Conceptualization. **Silvana Di Sabatino:** Writing – review & editing, Supervision, Project administration, Funding acquisition.

Declaration of competing interest

The authors declare that they have no known competing financial interests or personal relationships that could have appeared to influence the work reported in this paper.

Acknowledgements

This work received financial support under the National Recovery and Resilience Plan (NRRP), Mission 4, Component 2, Investment 1.1, Call for tender No. 104 published on 2.2.2022 by the Italian Ministry of University and Research (MUR), funded by the European Union – NextGenerationEU. Project Title “*Multi-scale investiGation of natuRe-basEd solutions for thE mitigation of urban heat and POLLution ISland (GREEN-POLIS)*” authorised by MUR – CUP J53D23002560001 - Grant Assignment Decree No. 20224HHCK7_001. The authors acknowledge the use of computational resources from the parallel computing cluster of the Open Physics Hub at the Department of Physics and Astronomy “Augusto Righi” at the University of Bologna (Italy). This work has also received support from the TRIGGER project funded by the European Union’s Horizon 2020 Research and Innovation programme, under the Grant Agreement number 822735.

Appendix A. Visualisation of computational mesh structures

Fig. A.17 illustrates the computational mesh structure used in the present study. Panel (a) shows the smooth-roof case, while panel (b) displays the case with a tree crown, where local refinement around the vegetation domain is visible.

Table B.2
The mean recirculation quotient defined in Eq. (B.1).

Simulation case	Φ
Without tree	0.6102
Dense LAI 8	0.6139
Dense LAI 11	0.5955
Linear LAI 8	0.5917
Linear LAI 11	0.601
Power LAI 8	0.5805
Power LAI 11	0.5812
Constant profile LAI 8	0.6054
Constant profile LAI 11	0.6018

Appendix B. Pollutant removal from the canyon

The pollutant concentration is used to quantify the overall fluid recirculation in the canyon. Following Göthe et al. (1988), the mean recirculation quotient is defined as

$$\Phi = \int_{\text{canyon}} \langle C^* \rangle dV / \int_{\text{domain}} \langle C^* \rangle dV, \quad (\text{B.1})$$

where C^* is the non-dimensional concentration averaged in time and space, integrated on the canyon volume (numerator) and on the entire domain (denominator). The quotients for the cases simulated are reported in Eq. (B.1). Across all cases, the maximum relative difference in Φ was found to be 5%, indicating that rooftop trees cause only marginal changes in overall pollutant retention within the canyon (see Table B.2).

To contextualise the above differences for real-world application, the maximum relative variation (5% in the mean recirculation quotient Φ) is expressed against each pollutant air-quality guideline values. A single combined air-quality limit across pollutants is not defined in WHO guidelines or EU legislation; compliance is assessed for each pollutant separately. Therefore, the observed 5% variation is contextualised against each standard individually. Using the WHO (World Health Organization, 2021) guidelines, 5% corresponds to $0.75 \mu\text{g m}^{-3}$ for the daily $\text{PM}_{2.5}$ guideline ($15 \mu\text{g m}^{-3}$), $2.25 \mu\text{g m}^{-3}$ for daily PM_{10} ($45 \mu\text{g m}^{-3}$), and $1.25 \mu\text{g m}^{-3}$ for daily NO_2 ($25 \mu\text{g m}^{-3}$). Using EU legislation, 5% of the 2030 daily limits given in Directive (EU) 2024/2881 (European Union, 2024) equals $1.25 \mu\text{g m}^{-3}$ for $\text{PM}_{2.5}$ ($25 \mu\text{g m}^{-3}$), $2.25 \mu\text{g m}^{-3}$ for PM_{10} ($45 \mu\text{g m}^{-3}$), and $2.50 \mu\text{g m}^{-3}$ for NO_2 ($50 \mu\text{g m}^{-3}$). These values indicate that a 5% difference lies below the magnitude of the respective daily or annual standards.

Data availability

Data will be made available on request.

References

- Abhijith, K.V., Gokhale, Sharad, 2015. Passive control potentials of trees and on-street parked cars in reduction of air pollution exposure in urban street canyons. *Environ. Pollut.* 204, 99–108.
- Balczó, Márton, Gromke, Christof, Ruck, Bodo, 2009. Numerical modeling of flow and pollutant dispersion in street canyons with tree planting. *Meteorol. Z.* 18 (2), 197.
- Baratian-Ghorghi, Z., Kaye, Nigel B., 2013. The effect of canyon aspect ratio on flushing of dense pollutants from an isolated street canyon. *Sci. Total Environ.* 443, 112–122.
- Biswal, Basanta Kumar, Bolan, Nanthi, Zhu, Yong-Guan, Balasubramanian, Rajasekhar, 2022. Nature-based systems (nbs) for mitigation of stormwater and air pollution in urban areas: A review. *Resour. Conserv. Recycl.* 186, 106578.
- Brown, M., Lawson, R., DeCroix, D., Lee, R., 2000. Mean flow and turbulence measurements around a 2-d array of buildings in a wind tunnel, 11th ams appl. of air poll. In: *Meteor. Conf.*
- Byoungchull, Oh, Beungyong, Park, 2024. Cfd analysis of the impact of building layout and morphology on pedestrian-level airflow and pollutant stagnation in urban areas with well-developed surface boundary layers. *Sustainability* 16 (13), 5745.
- Chen, Xiaoping, Wang, Xiaoshuang, Wu, Xiaogang, Guo, Jinping, Zhou, Zhixiang, 2021. Influence of roadside vegetation barriers on air quality inside urban street canyons. *Urban For. Urban Green.* 63, 127219.
- Chew, Lup Wai, Aliabadi, Amir A., Norford, Leslie K., 2018. Flows across high aspect ratio street canyons: Reynolds number independence revisited. *Environ. Fluid Mech.* 18, 1275–1291.
- Cintolesi, Carlo, Barbano, Francesco, Trudu, Pier Luigi, Finco, Angelo, Gerosa, Giacomo, Di Sabatino, Silvana, 2023. Characterisation of flow dynamics within and around an isolated forest, through measurements and numerical simulations. *Agricult. Forest. Meteorol.* 339, 109557.
- Cintolesi, Carlo, Petronio, A., Armenio, Vincenzo, 2015. Large eddy simulation of turbulent buoyant flow in a confined cavity with conjugate heat transfer. *Phys. Fluids* 27 (9).
- Cintolesi, Carlo, Pulvirenti, Beatrice, Di Sabatino, Silvana, 2021. Large-eddy simulations of pollutant removal enhancement from urban canyons. *Bound.-Layer Meteorol.* 180, 79–104.
- Dalpé, B., Masson, Christian, 2009. Numerical simulation of wind flow near a forest edge. *J. Wind Eng. Ind. Aerodyn.* 97 (5–6), 228–241.
- Di Paola, Lucia, 2021. Milan's private vertical forests vs. horizontal urban greening. In: *The Green City and Social Injustice*. Routledge, pp. 25–34.
- Di Sabatino, Silvana, Buccolieri, Riccardo, Kumar, Prashant, 2018. Spatial distribution of air pollutants in cities. In: *Clinical Handbook of Air Pollution-Related Diseases*. pp. 75–95.

- Dubief, Yves, Delcayre, Franck, 2000. On coherent-vortex identification in turbulence. *J. Turbul.* 1 (1), 011.
- Endalew, A. Melese, Hertog, Maarten, Delele, M.A., Baetens, K., Persoons, Tim, Baelmans, Martine, Ramon, Herman, Nicolai, B.M., Verboven, Pieter, 2009. Cfd modelling and wind tunnel validation of airflow through plant canopies using 3d canopy architecture. *Int. J. Heat Fluid Flow* 30 (2), 356–368.
- European Union, 2024. Directive (eu) 2024/2881 of the european parliament and of the council of 23 october 2024 on ambient air quality and cleaner air for europe.
- Gallagher, John, Baldauf, Richard, Fuller, Christina H., Kumar, Prashant, Gill, Laurence W., McNabola, Aonghus, 2015. Passive methods for improving air quality in the built environment: A review of porous and solid barriers. *Atmos. Environ.* 120, 61–70.
- Ghasemian, Masoud, Amini, Seyedmorteza, Princevac, Marko, 2017. The influence of roadside solid and vegetation barriers on near-road air quality. *Atmos. Environ.* 170, 108–117.
- Göthe, Carl-Johan, Bjurström, Rasmus, Ancker, Klas, 1988. A simple method of estimating air recirculation in ventilation systems. *Am. Ind. Hyg. Assoc. J.* 49 (2), 66–69.
- Gromke, Christof B., Blocken, Bert J.E., 2014. Implications of vegetation on pollutant dispersion in an idealized urban neighborhood. In: *Air Pollution Modeling and Its Application XXIII*. Springer, pp. 427–431.
- Gromke, Christof, Blocken, Bert, 2015a. Influence of avenue-trees on air quality at the urban neighborhood scale. part i: Quality assurance studies and turbulent schmidt number analysis for rans cfd simulations. *Environ. Pollut.* 196, 214–223.
- Gromke, Christof, Blocken, Bert, 2015b. Influence of avenue-trees on air quality at the urban neighborhood scale. part ii: Traffic pollutant concentrations at pedestrian level. *Environ. Pollut.* 196, 176–184.
- Guo, Yayun, Xiao, Qiankun, Ling, Chen, Teng, Mingjun, Wang, Pengcheng, Xiao, Zhiyan, Wu, Changguang, 2023. The right tree for the right street canyons: An approach of tree species selection for mitigating air pollution. *Build. Environ.* 245, 110886.
- Gurjão, Nayara de Oliveira, Júnior, Jorge Luiz Oliveira Lucas, Furtado, Lara Sucupira, Barbosa, Jorge Soares, 2024. Air pollution dynamics in fortaleza, brazil: Exploring the interplay of traffic and high-rise development. *Urban Clim.* 58, 102176.
- Irga, P.J., Burchett, M.D., Torpy, F.R., 2015. Does urban forestry have a quantitative effect on ambient air quality in an urban environment? *Atmos. Environ.* 120, 173–181.
- Jasak, Hrvoje, Weller, H.G., Gosman, A.D., 1999. High resolution nvd differencing scheme for arbitrarily unstructured meshes. *Internat. J. Numer. Methods Fluids* 31 (2), 431–449.
- Jeanjean, Antoine P.R., Hinchliffe, G., McMullan, W.A., Monks, Paul S., Leigh, Roland J., 2015. A cfd study on the effectiveness of trees to disperse road traffic emissions at a city scale. *Atmos. Environ.* 120, 1–14.
- Jiménez, M. Soledad, Cermák, Jan, Kucera, Jiri, Morales, Domingo, 1996. Laurel forests in tenerife, canary islands: the annual course of sap flow in laurus trees and stand. *J. Hydrol.* 183 (3–4), 307–321.
- Kalogeropoulos, Georgios, Tzortzi, Julia, Dimoudi, Argiro, 2024. Remote sensing and field measurements for the analysis of the thermal environment in the “bosco verticale” area in milan city. *Land* 13 (2), 182.
- Kang, Geon, Kim, Jae-Jin, Choi, Wonsik, 2020. Computational fluid dynamics simulation of tree effects on pedestrian wind comfort in an urban area. *Sustain. Cities Soc.* 56, 102086.
- Katul, Gabriel, Albertson, John D., 1998. An investigation of higher-order closure models for a forested canopy. *Bound.-Layer Meteorol.* 89, 47–74.
- Li, Xian-Xiang, Leung, Dennis Y.C., Liu, Chun-Ho, Lam, Kit Ming, 2008. Physical modeling of flow field inside urban street canyons. *J. Appl. Meteorol. Clim.* 47 (7), 2058–2067.
- Marcolla, Barbara, Pitacco, Andrea, Cescatti, A., 2003. Canopy architecture and turbulence structure in a coniferous forest. *Bound.-Layer Meteorol.* 108, 39–59.
- McMullan, W.A., Angelino, Matteo, 2022. The effect of tree planting on traffic pollutant dispersion in an urban street canyon using large eddy simulation with a recycling and rescaling inflow generation method. *J. Wind Eng. Ind. Aerodyn.* 221, 104877.
- Meroney, Robert N., Pavageau, Michel, Rafailidis, Stilianos, Schatzmann, Michael, 1996. Study of line source characteristics for 2-d physical modelling of pollutant dispersion in street canyons. *J. Wind Eng. Ind. Aerodyn.* 62 (1), 37–56.
- Michioka, Takenobu, Sato, Ayumu, Takimoto, Hiroshi, Kanda, Manabu, 2011. Large-eddy simulation for the mechanism of pollutant removal from a two-dimensional street canyon. *Bound.-Layer Meteorol.* 138, 195–213.
- Moradpour, Maryam, Hosseini, Vahid, 2020. An investigation into the effects of green space on air quality of an urban area using cfd modeling. *Urban Clim.* 34, 100686.
- Moser-Reischl, Astrid, Franceschi, Eleonora, Rahman, Mohammad A., Rodrigues-Leite, Julia, Pretzsch, Hans, Pauleit, Stephan, Rötzer, Thomas, 2025. Spatial and temporal dynamics of the leaf area index (lai) of selected tree species in urban environments. *Urban For. Urban Green.* 107, 128795.
- Neinavaz, Elnaz, Skidmore, Andrew K., Darvishzadeh, Roshanak, Groen, Thomas A., 2016. Retrieval of leaf area index in different plant species using thermal hyperspectral data. *ISPRS J. Photogramm. Remote Sens.* 119, 390–401.
- Nosek, Štěpán, Fuka, Vladimír, Radović, Jelena, Babuková, Zuzana, Jaňour, Zbyněk, 2025. Can deeper street canyons ventilate better? an analysis of roof geometries and aspect ratios with a focus on pollutant dynamics. *Build. Environ.* 270, 112528.
- Ono, Azusa, Nozu, Tsuyoshi, 2024. Comparison between wind tunnel experiment and large-eddy simulation of concentration fluctuations in pollutant dispersion in a realistic urban area. *J. Wind Eng. Ind. Aerodyn.* 253, 105832.
- Ortiz, A.G., Guerreiro, C. De Brito Beirao, 2020. Air Quality in Europe-2020. European Environmental Agency, Copenhagen, Denmark.
- Pavageau, Michel, Schatzmann, Michael, 1999. Wind tunnel measurements of concentration fluctuations in an urban street canyon. *Atmos. Environ.* 33 (24–25), 3961–3971.
- Pinard, Denis Joseph Jean-Paul, 2002. Numerical simulation of wind in plant canopies.
- Poh, Hee Joo, Chan, Woei Leong, Wise, Daniel J., Lim, Chi Wan, Khoo, Boo Cheong, Gobeawan, Like, Ge, Zhengwei, Eng, Yong, Peng, Jia Xin, Raghavan, Venugopalan S.G., et al., 2020. Wind load prediction on single tree with integrated approach of l-system fractal model, wind tunnel, and tree aerodynamic simulation. *AIP Adv.* 10 (7).
- Pope, Stephen B., 2001. Turbulent flows. *Meas. Sci. Technol.* 12 (11), 2020–2021.
- Qin, Peng, Ricci, Alessio, Blocken, Bert, 2024. On the accuracy of idealized sources in cfd simulations of pollutant dispersion in an urban street canyon. *Build. Environ.* 265, 111950.
- Ren, Feihong, Qiu, Zhaowen, Liu, Zhen, Bai, Hua, Gao, H. Oliver, 2023. Trees help reduce street-side air pollution: A focus on cyclist and pedestrian exposure risk. *Build. Environ.* 229, 109923.
- Rodi, Wolfgang, Constantinescu, George, Stoesser, Thorsten, 2013. Large-eddy simulation in hydraulics.
- Safayet, Mastura, Arefin, Md. Faqul, Hasan, Md. Musleh Uddin, 2017. Present practice and future prospect of rooftop farming in dhaka city: A step towards urban sustainability. *J. Urban Manag.* 6 (2), 56–65.
- Sagaut, Pierre, 2005. Large Eddy Simulation for Incompressible Flows: An Introduction. Springer Science & Business Media.
- Salim, Salim Mohamed, Buccolieri, Riccardo, Chan, Andrew, Di Sabatino, Silvana, 2011. Numerical simulation of atmospheric pollutant dispersion in an urban street canyon: Comparison between rans and les. *J. Wind Eng. Ind. Aerodyn.* 99 (2–3), 103–113.
- Santiago, Jose-Luis, Rivas, Esther, Sanchez, Beatriz, Buccolieri, Riccardo, Esposito, Antonio, Martilli, Alberto, Vivanco, Marta G., Martin, Fernando, 2022. Impact of different combinations of green infrastructure elements on traffic-related pollutant concentrations in urban areas. *Forests* 13 (8), 1195.
- Shen, Jiaowen, Cui, Pengyi, Huang, Yuandong, Wu, Yiping, Luo, Yang, Sin, Chung Hyok, Guan, Jie, 2023. New insights on precise regulation of pollutant distribution inside a street canyon by different vegetation planting patterns. *Environ. Sci. Pollut. Res.* 30 (22), 63148–63174.

- Smagorinsky, Joseph, 1963. General circulation experiments with the primitive equations: I. the basic experiment. *Mon. Weather Rev.* 91 (3), 99–164.
- Tallis, Matthew, Taylor, Gail, Sinnett, Danielle, Freer-Smith, Peter, 2011. Estimating the removal of atmospheric particulate pollution by the urban tree canopy of London, under current and future environments. *Landsc. Urban Plan.* 103 (2), 129–138.
- The OpenFOAM Foundation, 2018. OpenFOAM (version 6.0). <http://openfoam.org>. (Accessed 12 February 2025).
- Tominaga, Yoshihide, Stathopoulos, Ted, 2013. CFD simulation of near-field pollutant dispersion in the urban environment: A review of current modeling techniques. *Atmos. Environ.* 79, 716–730.
- Wang, Zixuan, Li, Yuguo, Song, Jiyun, Wang, Kai, Xie, Jing, Chan, Pak Wai, Ren, Chao, Di Sabatino, Silvana, 2022. Modelling and optimizing tree planning for urban climate in a subtropical high-density city. *Urban Clim.* 43, 101141.
- Wang, Xiaoshuang, Zhou, Zhixiang, Xiang, Yang, Peng, Chucai, Peng, Changhui, 2024. Effects of street plants on atmospheric particulate dispersion in urban streets: A review. *Environ. Rev.* 32 (1), 114–130.
- World Health Organization, 2021. WHO global air quality guidelines: Particulate matter (PM_{2.5} and PM₁₀), ozone, nitrogen dioxide, sulfur dioxide and carbon monoxide.
- World Health Organization, 2025. Ambient (outdoor) air quality and health. [https://www.who.int/news-room/fact-sheets/detail/ambient-\(outdoor\)-air-quality-and-health](https://www.who.int/news-room/fact-sheets/detail/ambient-(outdoor)-air-quality-and-health). (Accessed 09 January 2025).
- Xu, Tao, Zhou, Hao, Lv, Xiaolan, Lei, Xiaohui, Tao, Shutian, 2022. Study of the distribution characteristics of the airflow field in tree canopies based on the CFD model. *Agronomy* 12 (12), 3072.
- Zeng, Fanxing, Lei, Chengwang, Liu, Jianlin, Niu, Jianlei, Gao, Naiping, 2020. CFD simulation of the drag effect of urban trees: Source term modification method revisited at the tree scale. *Sustain. Cities Soc.* 56, 102079.
- Zhang, Wei-Chen, Luo, Xiang-Yu, Peng, Xin-Ru, Liu, Run-Zhe, Jing, Yi, Zhao, Fu-Yun, 2021. Green roof on the ventilation and pollutant dispersion in urban street canyons under unstable thermal stratification: Aiding and opposing effects. *Sustain. Cities Soc.* 75, 103315.